An Adaptive Threshold Detector and Channel Parameter Estimator for Deep Space Optical Communications

R. Mukai, P. Arabshahi, T.-Y. Yan
Jet Propulsion Laboratory
4800 Oak Grove Drive, MS 238–343
Pasadena, CA 91109 USA
[mukai,payman,yan]@jpl.nasa.gov

Abstract— **A method for optimal adaptive setting of pulse-position-modulation pulse detection thresholds, which minimizes the total probability of error for the dynamically fading optical free space channel, is presented. The threshold's adaptive setting, in response to varying channel conditions, results in orders of magnitude improvement in probability of error, as compared to use of a fixed threshold. The adaptive threshold system itself is based on a robust channel identification system that uses average signal strengths to estimate the degree of fade and total attenuation in the channel, and a radial basis function network for estimating pulse spreads, all with excellent accuracy.**

I. Introduction

Over the past years, NASA and JPL have continuously sought to reduce spacecraft size and mass while increasing its information return capability. Laser communications provide a way of achieving this goal. The highly collimated beam allows for significant reductions in the size and mass of the communications terminal along with reduced power requirements. Optical communications also avoids problems involving radio frequency resource and spectrum allocation, interference, and frequency and bandwidth regulation. Since an increasing number of missions will operate at high downlink data rates, the avoidance of these issues is a significant advantage.

The optical communication system under study at JPL uses pulse-position modulation (PPM) to transmit data. Each PPM symbol consists of 256 signal slots of 20 ns each, followed by approximately 15 μs of "dead time" (see Fig. 1). The "dead-time" is present to allow the Q-switched laser sufficient charging time between pulses. Within the slot, there is a small (2 ns) guard time on each side of the 16 ns duration pulse to provide a safety margin against pulse jitter associated with Q-switched lasers [1], [2].

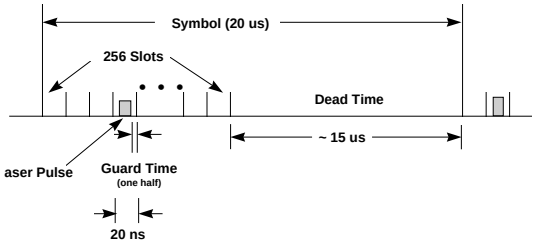

Fig. 1. Pulse Position Modulation timing diagram: the slot width T_s is 20 ns; the symbol width T_l is 20 μs; there are $N_s = 256$ slots in a symbol, within which a signal pulse can occur; there are $N_d \approx 750$ dead-time slots in a symbol; and there are about one thousand ($N_s + N_d$) total slots per symbol.

The research described in this publication was carried out as part of a task funded by the *Technology and Applications Program* (TAP) at the Jet Propulsion Laboratory, California Institute of Technology, under a contract with the National Aeronautics and Space Administration.

Space-based optical communication systems are subject to several factors which can impact their performance. Changes in atmospheric conditions on Earth can cause time-smearing, fading, and changes in the received pulse shape [3]. Furthermore, laser communication systems are sensitive to pointing errors, which can cause deep signal fades. As a result, the problem of detecting and acquiring PPM signals under varying channel conditions is a major challenge. If it is known a priori that a PPM symbol does exist, then it is known that the optimal strategy for demodulation is to pick the maximum slot value [4], [5]. However, the problem of initially detecting and acquiring the signal poses a greater challenge since selecting the maximum slot value simply yields a random number if no signal is present.

To address this problem, an adaptive threshold device can be employed to eliminate the "noise-only" case, and assist in the problem of detection and acquisition of the PPM signal. Such a device is a component of an overall "intelligent agent", which, additionally, assists in slot and frame synchronization, control of the phase-locked loop, and determination of channel conditions and characteristics [1], [6].

The signal detection threshold is set based on information received from the intelligent agent, in the form of extracted channel parameters (in turn obtained by analyzing the output of an initial avalanche photodiode detector – APD). We will discuss the design and testing of both the channel parameter identification system, and the adaptive threshold system, in this paper, and illustrate advantages and performance gains obtained under simulated channel degradation conditions.

II. Pulse Modeling

It is common for optical pulses to assume Gaussian or exponentially decaying shapes [3], [7] in the time-domain. An ideal Gaussian pulse is described by

$$E\left[x(t)\right] = \alpha \frac{n_s}{\sigma\sqrt{2\pi}} \exp\left(-\frac{(t-t_0)^2}{2\sigma^2}\right), \qquad (1)$$

where n_s is the average number of signal photons in the signal pulse, σ is the time-domain spread of the pulse, t_0 is the center of the pulse in the time-domain, and α is the multiplicative fade, assumed to be a constant. An ideal exponential pulse with time constant τ is described by

$$E\left[x(t)\right] = \left(\alpha n_s/\tau\right) \exp\left(-t/\tau\right) \qquad (2)$$

Eight different pulse types and spreads (four Gaussian and four exponential) corresponding to eight hypotheses were considered, as defined in Table I. Hypotheses H_1 and H_5 correspond to "half-width" pulses, which are one-half the normal width. Hypotheses H_2 and H_6 correspond to "full-width" pulses in which 99% of the photons are contained within the 20 ns slot duration. Hypotheses H_3 and H_7 correspond to

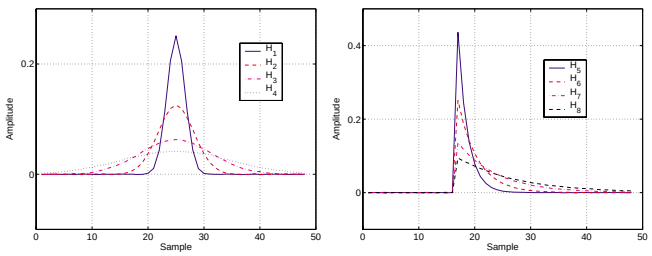

Fig. 2. Illustration of Gaussian (left), and exponential (right) pulse shapes used in the simulations. The sampling rate is 800 MHz (16 samples per 20 ns slot). For the Gaussian pulses, three PPM slots (48 samples) are illustrated with the signal slot in the center. The exponential pulses begin at the start of the signal slot in order to maximize photon collection within the signal slot.

"double-width" pulses containing 99% of their photons within two PPM slots, and hypotheses H_4 and H_8 correspond to "triple-width" pulses in which 99% of the photons are spread over three slots. In the exponentially decaying case the pulse is defined to start at the beginning of the slot (to catch the largest number of photons in the signal slot), while in the Gaussian case the pulse is centered at the middle of the signal slot (once again to maximize the number of photons in the signal slot itself). Figure 2 illustrates the four Gaussian and exponential pulse types tested.

Hypothesis (Gaussian)	σ	Hypothesis (Exponential)	τ
H_1	$0.1T_s$	H_5	$0.5T_s/\ln(100)$
H_2	$0.2T_s$	H_6	$T_s/\ln(100)$
H_3	$0.4T_s$	H_7	$2T_s/\ln(100)$
H_4	$0.6T_s$	H_8	$3T_s/\ln(100)$

TABLE I

HYPOTHESES AND PULSE SHAPES CORRESPONDING TO FIG. 2.

The attenuation of the signal can be modeled by another multiplicative parameter β, which is a function of α and σ for Gaussian pulses; and α and τ for exponential pulses.

Once σ, α, and β are known, or adaptively estimated, they can be used in conjunction with receiver operating characteristic (ROC) curves to adaptively select the optimum signal detection threshold, λ, for minimizing the total error probability.

A. Estimating pulse spread

Neural networks are commonly used to solve problems in pattern recognition [8]. We use a radial basis function network here to recognize pulse shapes, with particular emphasis on determining the pulse spread σ or τ, via the following steps:

1. Noise-only portions of the received PPM symbols (i.e. the "dead-slots") are averaged to compute the ambient background signal. This DC background level is subtracted out, removing daylight effects, and leaving us with only the received signal pulse; thus simplifying the analysis.
2. The vector of pulse samples is normalized to unit L_1 norm. A great deal of training time can be saved if the neural network is presented with normalized pulse shapes. This improves system reliability as well since the network is less likely to be confused by differences in the pulse caused by fading.
3. The normalized pulse is presented to the neural network for analysis. The network returns a number indicating its estimate of the pulse spread parameter σ for a Gaussian pulse or the time-decay parameter τ for an exponential pulse.

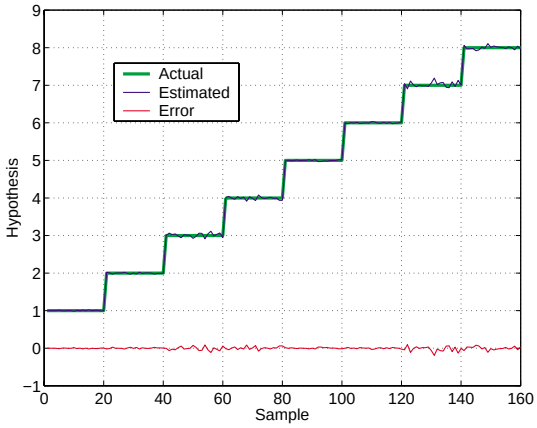

Fig. 3. Classification performance of the RBF network without pulse fading. The light gray line denotes actual pulse categories and the darker line denotes the network's classification output. The error is also illustrated.

Additional performance gains can be obtained by using a Reed-Solomon (255,223) code to encode the data in order to detect and remove defective PPM symbols, or possible shot noise events. A total of 255 received symbols are decoded to obtain 223 original data symbols. These are then re-encoded, and the resulting 255 "corrected" symbols are compared to the symbols received from the channel. Any channel symbols differing from the results of re-encoding are considered to be noise events and are ignored. Symbols agreeing with the re-encoded symbols are deemed reliable, and used in the average.

For each symbol to be averaged, five slots (80 samples) consisting of the received PPM signal pulse and its adjacent slots are selected. An average pulse consisting of up to 255 received channel pulses is thus computed. Forty-eight samples, corresponding to the three central slots, are presented to the RBF network for classification since the 32 side samples contain little information of use to the neural network. This procedure results in more reliable averaged symbols being presented to the RBF network, allowing very accurate pulse classification.

Figure 3 illustrates the ability of the RBF network to classify pulses based on their pulse spreads. The actual pulse categories and the neural network's classification output are seen to be very close to each other, demonstrating the network's excellent classification accuracy and low error performance.

B. Estimating pulse fade α

The fade α of the slot signal is a linear function of the L_1 norm of the pulse. Since the pulse vector consists of 80 samples, corresponding to 5 slots, the L_1 norm of the pulse is not significantly affected by pulse smearing even for fairly large pulse spreads. Let C_0 denote the average signal charge released by the APD over five slots under ideal conditions, (i.e. no attenuation caused by fading or by scintillation). Let C denote the average charge actually received over the five slots. The background daylight level is removed from both C_0 and C. The fade estimate is then given by:

$$\alpha = C/C_0 \tag{3}$$

Figure 4 illustrates the ability of the system to estimate fades once the pulse spread σ is known. The estimated fades are plotted against actual fades, and it can be seen that the points lie close to the line $y = x$, indicating the estimator's accuracy.

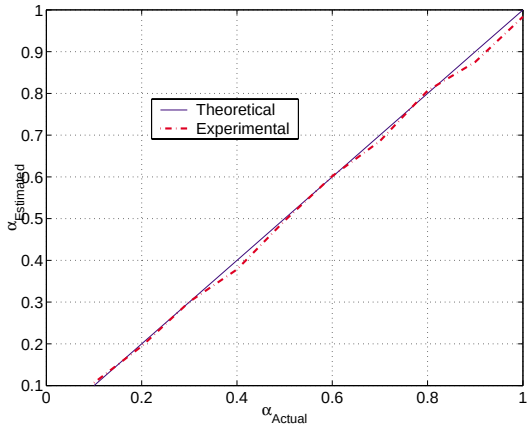

Fig. 4. Fade estimation performance for a Gaussian pulse with $\sigma = 0.2T_s$, and $\alpha = 0.10 - 1.00$ under daytime conditions.

C. Determining pulse attenuation β

In addition to the multiplicative fade α caused by the channel, scintillation causes photons to be spread outside of the main signal slot, causing further attenuation. Let x_0 denote the nominal slot signal from the APD due only to signal photons in the case where fading and scintillation are not significant. Let x denote the actual average APD slot output due to signal photons only under actual operating conditions. Note that the DC background due to ambient light has already been subtracted away in both x_0 and x. The best (maximum likelihood) estimate of β is then given by:

$$\beta = x/x_0 \tag{4}$$

Note that Eq. (3) is based on summation over five slots when calculating C and C_0. By contrast, Eq. (4) is based on summation over only one slot (the signal slot). β is thus a measure of signal strength only within the PPM slot containing the signal pulse. α, by contrast, is a measure of signal strength which includes any photons which have been spread to slots adjoining the main signal slot. Since α is a more inclusive measure, it is affected little by pulse spread. By contrast, even in the absence of any multiplicative fade, β can be greatly reduced if a wide pulse spreads its photons into other PPM slots.

There exists a relationship between β and α. The total multiplicative attenuation β of a Gaussian pulse can be written as

$$\beta = \alpha f(\sigma), \tag{5}$$

where $f(\sigma)$ is the average proportion of "signal photons" contained in the signal slot. This is derived to be

$$f(\sigma) = \int_{-\frac{T_s}{2}}^{\frac{T_s}{2}} \frac{1}{\sigma\sqrt{2\pi}} \exp\left(-\frac{t^2}{2\sigma^2}\right) dt = 1 - 2Q\left(\frac{T_s}{2\sigma}\right), \tag{6}$$

and thus

$$\beta = \alpha\left[1 - 2Q\left(\frac{T_s}{2\sigma}\right)\right], \tag{7}$$

as expressed in terms of the commonly used "Q" function in communications. [1]

In the case of an exponential pulse (Eq. (2)), we define the pulse duration as the time T_d which contains, on average, 99% of the photons in the pulse. This yields $\tau = T_d/\ln(100)$ as the pulse's time constant.

[1] $Q(x) = \sqrt{2\pi}^{(-1)} \int_x^\infty \exp(-t^2/2)dt$

Given τ, we compute the average fraction of signal photons in a slot by computing

$$\frac{\int_0^{T_s} \exp(-t/\tau)\, dt}{\int_0^\infty \exp(-t/\tau)\, dt} = 1 - \exp(-T_s/\tau) = 1 - (0.01)^{\frac{T_s}{T}} \tag{8}$$

which in turn yields the following for β:

$$\beta = \alpha\left[1 - (0.01)^{\frac{T_s}{T_d}}\right] = \alpha\left(1 - \exp\left(-\frac{T_s}{\tau}\right)\right). \tag{9}$$

It is possible to use either Eq. (7) or (9) to compute β for the corresponding cases. We will use Eq. (4) for both cases here.

III. Pulse Detection

Starting with estimates of the above parameters at regular time intervals, the next step in determining the signal detection threshold is to compute the receiver operating characteristic (ROC) curves.

Let P_{FA} be the probability of false alarm. This is the probability that APD noise will exceed the signal detection threshold, thus causing a PPM symbol detection event when no PPM symbol exists. Let P_D be the probability of successful signal detection, which is the probability that if a pulse is present it will be successfully detected. The two hypotheses are therefore: ξ_0, the hypothesis under which no pulse has been sent; and ξ_1, the hypothesis under which a pulse has been sent.

Let $p(x|\xi_0)$ denote the probability density function (pdf) of the received slot signal x given hypothesis ξ_0 and $p(x|\xi_1)$ denote the pdf of the received slot signal x given hypothesis ξ_1. P_{FA} and P_D are then given in terms of the threshold λ as:

$$P_{FA}(\lambda) = \int_\lambda^\infty p(x|\xi_0)dx \tag{10}$$

$$P_D(\lambda) = \int_\lambda^\infty p(x|\xi_1)dx \tag{11}$$

Equations (10) and (11) are used to compute the ROC curve for this receiver - parameterized by λ for a given set of channel conditions - as a plot of P_D versus P_{FA}.

The significance of the ROC lies in the calculation of error probabilities P_e. An error is either a false alarm or a missed detection. P_e as a function of λ is given by:

$$P_e(\lambda) = P(\xi_0)P_{FA}(\lambda) + P(\xi_1)(1 - P_D(\lambda)) \tag{12}$$

Using the parameterized values of P_{FA} and P_D from the ROC in conjunction with a priori probabilities, we can compute the probability of error as a function of the detection threshold λ, allowing the optimal threshold λ to be determined.

A. The use of β in selecting a ROC

Selection of an ROC to be used in Eq. (12) is made based on a corresponding estimated value for β. It is therefore reasonable to ask whether the use of an overall slot signal attenuation β for this purpose is justified. This can be an important issue if the time-domain spread of the pulse is unusually large, leading to significant presence of signal photons in slots adjacent to the signal slot. [2]

Experimental results, however, suggest that the ROC typically remains the same for constant β even when significant variations exist in both α and σ (α and τ for exponential pulses). This is illustrated in Fig. 5. In spite of significant differences in pulse shapes, the ROC is essentially a function of total signal slot attenuation β. These and other similar results justify the use of β in selecting an ROC curve, followed by the use of the ROC to compute P_e.

[2] This will not be the case for most typical values of σ or τ.

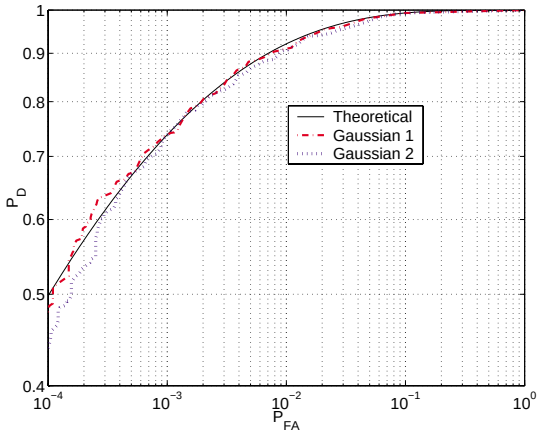

Fig. 5. Illustrated here are a "theoretical" ROC curve for $\beta = 0.2900$; and two experimentally obtained ROC curves: "Gaussian 1" for the case where $\sigma = 0.2T_s$ and $\alpha = 0.30$, corresponding to $\beta = 0.2963$, and "Gaussian 2" for the case where $\sigma = 0.6T_s$ and $\alpha = 0.50$, corresponding to $\beta = 0.2977$.

B. The issue of unknown a priori probabilities

In practice, a priori probabilities $P(\xi_0)$ and $P(\xi_1)$ in Eq. (12) are rarely known. To assess system performance, the minimax criterion may be used to determine a priori probabilities yielding the highest probability of error $P_e^*(\lambda)$. Figure 6 illustrates this worst case $P_e^*(\lambda)$ as a function of the total signal slot attenuation β and of the threshold λ. In Fig. 6, the threshold λ is expressed as a percentage of the maximum, defined as

$$\lambda_{\max} = 2q\eta G(n_s + n_b) \tag{13}$$

where q is the electron charge (1.6×10^{-19} C), η is the quantum efficiency of the APD (0.38 in our case), G is the average APD gain (40 in our case), n_s is the number of signal photons in a single pulse, and n_b is the number of background noise photons in a slot. $\lambda_{\max}$ was calculated separately for day and night cases since they involve different values of n_s and n_b.

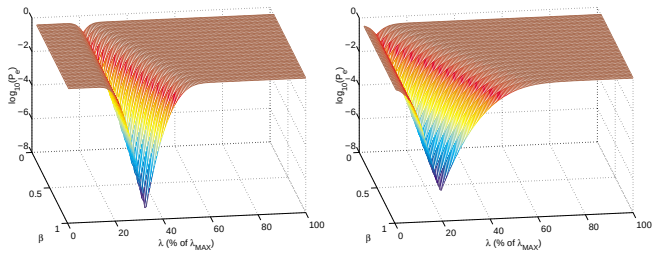

Fig. 6. $\log_{10}(P_e)$ as defined in Eq. (12) plotted as a function of the threshold λ and the multiplicative attenuation β for both day (left) and night (right) conditions, for the case of worst case a priori probabilities. The deep valley in the plot traces the path of the optimal threshold for different β. It can be seen that for lower values of β the optimal threshold is lower, while higher values of β require higher thresholds.

Figure 6 shows a deep valley in the plot of P_e^* versus both λ and β. This valley traces the optimal value of λ for a given β, clearly illustrating the critical need for the system to adapt its threshold as β changes.

IV. Experimental Results

A. Example 1: Gaussian pulse – daytime steady-state

Two sets of operating conditions are presented. Under the first set, signals are prepared with $\alpha = 0.5$, and $\sigma = 0.6$, yielding $\beta = 0.2977$. α and β are then estimated for the noisy channel, using Eqs. (3) and (4). They are found to be $\hat{\alpha} = 0.4898$ and $\hat{\beta} = 0.3037$, which are very close to true values.

Under the second set, the signals have $\alpha = 0.8$ and $\sigma = 0.2$, yielding $\beta = 0.7901$. α and β are similarly estimated and found to be $\hat{\alpha} = 0.7917$ and $\hat{\beta} = 0.7712$, once again very close to true values.

In both cases a (255,223) Reed-Solomon code was used to remove defective PPM symbols.

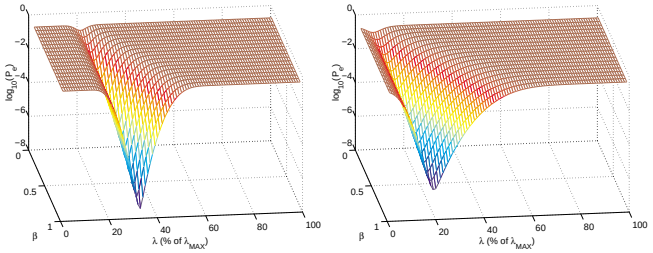

Fig. 7. $\log_{10}(P_e)$ as defined in Eq. (12) plotted as a function of the threshold λ and the multiplicative attenuation β for both day (left) and night (right) conditions, for the case of equal a priori probabilities. See also Fig. 6.

We can compute the theoretical error probabilities by using β for each case to select appropriate ROC curves. Assuming $P(\xi_0) = P(\xi_1) = 0.5$, the P_e surfaces can be computed (see Fig. 7). [3]

These can be cut along the $\beta = 0.2977$ and $\beta = 0.7901$ planes to obtain error probabilities as a function of the threshold λ (see Fig. 8). By choosing the minimum along the error probability lines, we can find the optimal threshold for the system. For the first case, where $\beta = 0.2977$, the opti-

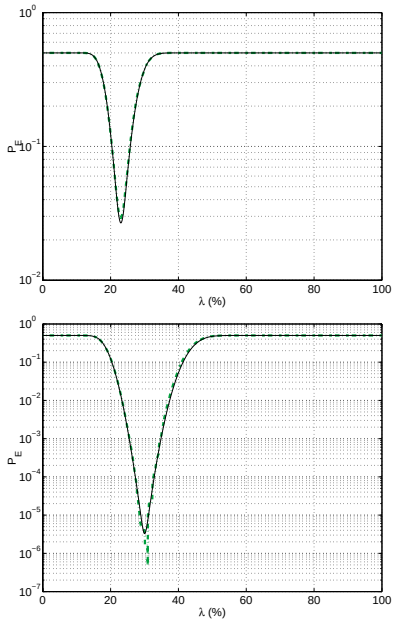

Fig. 8. Theoretical (solid) and experimental (dashed color) error probabilities for $\beta = 0.2977$ (top), and $\beta = 0.7901$ (bottom), assuming equal a priori probabilities and showing excellent agreement between the two. The mismatch near the trough of the curve on the right is due to an insufficient number of error events at the corresponding threshold.

[3] Note that the error surfaces are very similar to those for worst case minimax error probabilities (Fig. 6), making the equal a priori case a reasonable case for experimentation.

	$\beta = 0.2977$	$\beta = 0.7901$
$\lambda = 23.0\%$	2.76×10^{-2}	1.39×10^{-2}
$\lambda = 29.9\%$	0.374	4.06×10^{-6}

TABLE II

THEORETICAL P_e VALUES AS A FUNCTION OF THRESHOLD λ AND TOTAL ATTENUATION β FOR THE TWO DAYTIME CASES OF FADING.

	$\hat{\beta} = 0.3037$	$\hat{\beta} = 0.7712$
$\hat{\lambda} = 23\%$	2.92×10^{-2}	1.30×10^{-2}
$\hat{\lambda} = 31\%$	0.353	4.71×10^{-7}

TABLE III

EXPERIMENTAL P_e VALUES AS A FUNCTION OF THRESHOLD λ AND TOTAL ATTENUATION β FOR TWO DAYTIME CASES OF FADING.

	$\beta = 0.2970$	$\beta = 0.6930$
$\lambda = 9.5\%$	2.49×10^{-2}	9.74×10^{-3}
$\lambda = 15.0\%$	0.130	6.99×10^{-5}

TABLE IV

THEORETICAL P_e VALUES AS A FUNCTION OF THRESHOLD λ AND TOTAL ATTENUATION β FOR THE TWO NIGHT TIME CASES OF FADING.

	$\hat{\beta} = 0.2934$	$\hat{\beta} = 0.7043$
$\hat{\lambda} = 9.6\%$	1.87×10^{-2}	7.15×10^{-3}
$\hat{\lambda} = 16.0\%$	0.164	2.50×10^{-5}

TABLE V

EXPERIMENTAL P_e VALUES AS A FUNCTION OF THRESHOLD λ AND TOTAL ATTENUATION β FOR TWO NIGHT TIME CASES OF FADING.

mal threshold from the theoretical curve is found to be 23.0% (of $\lambda_{\max}$) with a $P_e = 2.76 \times 10^{-2}$. For the second case, where $\beta = 0.7901$, the optimal threshold is 29.9% with $P_e = 4.06 \times 10^{-6}$.

To illustrate the importance of changing the threshold as fading conditions change, consider the following scenarios.

For case I, with $\beta = 0.2977$, we set the threshold to its optimal value of 23%. Now if the threshold is not adapted as the channel changes to a state where $\beta = 0.7901$, (case II), P_e will approach 1.39×10^{-2}, which is nearly 4 orders of magnitude worse than the optimal value of $P_e = 4.06 \times 10^{-6}$ achievable by adjusting the threshold to 29.9%.

Similarly, let's say we start in case II with $\beta = 0.7901$; set the threshold to its optimal value of 29.9%; and then approach severe fading, causing β to fall to 0.2977 as in case I. If the threshold is not adapted to respond to this channel, we will have $P_e = 0.374$, which represents a greater than one in three chance of making an error. By contrast, adjusting the threshold down to 23.0% would reduce P_e to only 2.76×10^{-2}, which is less than a three-percent chance of error. This represents a full order of magnitude improvement in error probabilities resulting from threshold adjustment.

These results are summarized in Tables II and III. Excellent agreement between theoretical and simulated values of P_e and λ is observed. The discrepancy between experimental and theoretical P_e values for $\beta = 0.7901$ and $\lambda = 29.9\%$ is due to an insufficient number of error events in the simulations.

B. Example 2: Exponential pulse – night acquisition

Here only ten pulses are averaged for acquisition and rapid determination of channel parameters. No error control code is used to remove defective symbols. The relevant parameters are as follows. Case I: fade $\alpha = 0.30$, spread $\tau = T_s / \ln(100)$. Case II: fade $\alpha = 0.70$, spread $\tau = T_s / \ln(100)$.

Results similar in nature to Example 1 are obtained.

Tables IV and V illustrate the performance of the system. The need for threshold adaptation, and the dramatic improvement in error probability as a result of it are once again confirmed, as in Example 1.

V. CONCLUSIONS

A method for adaptive setting of PPM pulse detection thresholds has been presented. The optimal detection threshold so obtained minimizes the total probability of error (either false alarm or missed detection) under a wide range of channel conditions. Its adaptive setting, in response to varying channel conditions, results in *orders of magnitude improvement* in probability of error, as compared to use of a fixed threshold, and is critical for free space optical PPM systems operating under fading and scintillation.

The adaptive threshold system itself is based on a robust channel identification system that uses average signal strengths to estimate the degree of fade and total attenuation, and an RBF network for estimating pulse spreads, all with excellent accuracy.

The channel identification system presented here is currently being further developed and incorporated into the PPM synchronization subsystem to aid in slot and symbol synchronization, in addition to signal detection.

ACKNOWLEDGMENTS

The authors wish to express their thanks to Meera Srinivasan and Jon Hamkins for providing the original source code needed for parts of the simulations, and to Victor Vilnrotter for helpful discussions.

REFERENCES

[1] T.-Y. Yan and C.-C. Chen, "Design and development of a baseline deep space optical PPM transceiver," *Proc. SPIE*, vol. 3615, pp. 154-169, January 1999.

[2] V.A. Vilnrotter, M.K. Simon, and T.-Y. Yan, "The power spectrum of pulse-position modulation with dead time and pulse jitter," *The Telecommunications and Mission Operations Progress Report 42-133*, JPL, Pasadena, CA, May 15, 1998. http://tmo.jpl.nasa.gov/tmo/

[3] Edward A. Bucher, Robert M. Lerner, and Charles W. Niessen, "Some experiments on the propagation of light pulses through Clouds," *Proc. IEEE*, vol. 58, no. 10, pp. 1564-1567, October 1970

[4] M. Srinivasan and V. Vilnrotter, "Symbol-error probabilities for pulse-position modulation signaling with an avalanche photodiode receiver and gaussian thermal noise," *The Telecommunications and Mission Operations Progress Report 42-134*, JPL, Pasadena, CA, August 15, 1998. http://tmo.jpl.nasa.gov/tmo/

[5] M. Srinivasan and V. Vilnrotter, "Performance of the optimum receiver for pulse-position modulation signals with avalanche photodiode statistics," *The Telecommunications and Mission Operations Progress Report 42-133*, JPL, Pasadena, CA, May 15, 1998. http://tmo.jpl.nasa.gov/tmo/

[6] K. Rahnamai, P. Arabshahi, and T.-Y. Yan,"A computationally intelligent fast acquisition algorithm for deep space optical communications," *Proc. Int. Conf. Signal Processing Applications and Technology*, Toronto, Canada, Sept. 1998.

[7] R.M. Gagliardi and S. Karp, *Optical communications*, John Wiley and Sons, 1995.

[8] Simon Haykin, *Neural networks: a comprehensive foundation*, Prentice Hall, 1998.